IEEE Access
Multidisciplinary | Rapid Review | Open Access Journal

Received July 14, 2019, accepted July 25, 2019, date of publication July 29, 2019, date of current version August 14, 2019.

Digital Object Identifier 10.1109/ACCESS.2019.2931765

Compact Microwave and Millimeter-Wave Bandpass Filters Using LTCC-Based Hybrid Lumped and Distributed Resonators

GUANGXU SHEN[1,2], (Student Member, IEEE), WENQUAN CHE[1,2], (Senior Member, IEEE), AND QUAN XUE[1], (Fellow, IEEE)

[1]School of Electronic and Information Engineering, South China University of Technology, Guangzhou 510006, China
[2]Department of Communication Engineering, Nanjing University of Science and Technology, Nanjing 210094, China

Corresponding author: Quan Xue (eeqxue@scut.edu.cn)

This work was supported in part by the Guangdong Innovative and Entrepreneurial Research Team Program under Grant 2017ZT07X032, in part by the Guangdong Province Key Project of Science and Technology under Grant 2018B010115001, and in part by the National Natural Science Foundation of China under Grant 61571231.

ABSTRACT A novel class of low-temperature cofired ceramic (LTCC) bandpass filters (BPFs) is proposed in this paper, featuring of compact size and good filtering responses in both microwave and millimeter-wave (mm-wave) bands. By effectively merging the lumped elements and distributed effects, a modified LTCC-based hybrid lumped and distributed resonator (HLDR) is introduced. In detail, the lumped part of a LTCC interdigital capacitor and a high-impedance line is used to reduce circuit size, loss, and cross-talks. The distributed part, saying, the mutual couplings between adjacent HLDRs and to the ground, is used to improve the design flexibility and filtering performance for HLDR filters. With mutual couplings, the coupling matrix method can be applied. Furthermore, the frequency-variant mixed couplings between HLDRs are investigated, and coupling matrix method is improved by introducing a new coupling mechanism. Multiple transmission zeroes (TZs) are firstly realized with second-order in-line topology, but without adding cross-couplings or bandstop structures. To validate above design strategies, one *S*-band and one *Ka*-band second-order HLDR BPFs are simulated and measured, respectively. Very compact size, low loss, high-selectivity, and wide upper stopband are observed, especially in mm-wave range.

INDEX TERMS Bandpass filter (BPF), design method, microwave, millimeter-wave, mixed couplings, low-temperature cofired ceramic (LTCC).

I. INTRODUCTION

With the progressive development of modern wireless technology, more frequency spectrums in microwave and millimeter-wave (mm-wave) have been used. For example, *S*-band (3.5 GHz) and *Ka*-band (28 & 39 GHz) are for the fifth generation (5G) mobile communication [1]. *K*-band (24 GHz) and *V*-band (77 GHz) are employed for automotive radar sensors [2]. In future, high-performance bandpass filters (BPFs) in both microwave and mm-wave ranges are demanded, which are the essential devices to select signals in RF front-ends.

Under 6 GHz, different types of bandpass filters have been investigated. The surface/bulk acoustic wave (SAW/BAW) filters are widely used in the mobile terminals [3]. For the base stations, the waveguide or co-axial cavity filters are the common solution due to its high-power capacity [4]. As the operating frequency rises to higher frequency, many challenges have been brought up for the design of BPFs. For example, SAW/BAW filters are not feasible for millimeter wave applications till now [3]. The system-on-a-chip (SoC) and system-in-a-package (SiP) are the two common solutions for mm-wave systems. Therefore, the features of compact size and high integration are critically required, which are not easy for waveguide and substrate integrate waveguide (SIW) filters [5], [6]. In addition, low transmission loss is also important, but the insertion loss of microstrip (MSL) filter usually increase with higher frequency [7]–[13]. Moreover, stopband suppression is demanded from microwave to mm-wave bands, which is not easy for lumped

The associate editor coordinating the review of this manuscript and approving it for publication was Feng Lin.

TABLE 1. Potential design methods for millimeter-wave BPFs.

	SAW/ BAW BPFs [3]	Wave-guide BPFs [5]	SIW BPFs [6]	MSL BPFs [7]-[13]	Lumped BPFs [14]-[15]	**Pro-posed HLDR BPFs**
MM-wave application	×	√	√	○	√	√
Flexible bandwidth	×	×	○	√	√	√
Low loss	○	√	○	×	○	○
Compact size	√	×	×	○	√	√
Easy integration	○	×	○	√	√	√
Stopband suppression	√	√	○	○	×	○
High selectivity	√	√	○	○	×	○

√: good, ○: medium, ×: bad

filters [14], [15]. Aiming at mm-wave application, the properties of the existing filter design methods have been summarized, as shown in Table 1. As observed, it is indeed difficult to design an mm-wave filter with all the specifications well satisfied by using above methods.

To improve the filter performance, the idea of hybrid filter was presented by merging different design methods together. In [16], the microstrip and ridged waveguide were both used to realize a low-loss filter in K-band. In [17], the proposed hybrid resonator contained a series and a shunt resonance, which can introduce one more transmission zero (TZ). To realize miniaturization, the lumped chip capacitors were welded to microstrip resonators in [18] and [19]. In [20] and [21], the lumped and distributed elements were realized with same fabrication process for further miniaturization. In [22], the distributed stepped-impedance resonators (SIRs) were used to replace the lumped elements in a lumped filter, resulting in multiple TZs in the stopband. In summary, the lumped elements can help reduce circuit size of BPFs, while the distributed ones can improve filtering responses. However, it is still not easy to realize compact size and good filtering performance simultaneously [18]–[22]. To solve this issue, the investigation on the integrated design method of lumped and distributed elements is necessary.

In this paper, a new class of low-temperature cofired ceramic (LTCC) bandpass filters is proposed by using hybrid lumped and distributed resonators (HLDRs). Aiming at compact size and low loss, HLDR is composed of quasi-lumped LTCC capacitor and high-impedance microstrip section inductor, as shown in Fig. 1. Different from published lumped resonators, the distributed effects are also introduced and analyzed for HLDRs. In particular, the inter-connection of HLDRs are realized by mutual couplings. In this way, the coupling matrix method [7], [23] for distributed filters can be applied for HLDR filters, which can highly improve the design flexibility and filtering performance.

Furthermore, the classic coupling matrix method is further improved by introducing a new coupling mechanism to

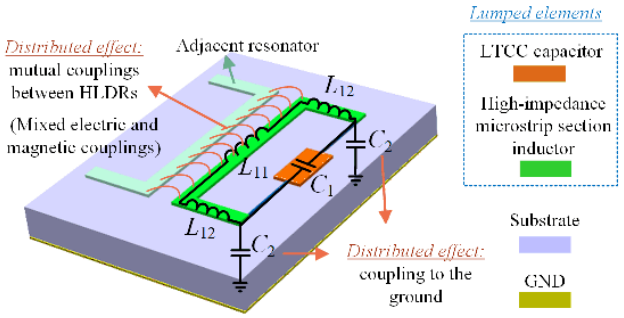

FIGURE 1. Topology of the proposed LTCC-based HLDR.

realize multiple TZs. Instead of cross couplings, the mixed electric and magnetic couplings are used for generating TZs. For HLDR filters, the mixed couplings are in-phase and frequency-variant, which can realize multiple TZs for HLDR filter, even with two-pole in-line topology. In detail, two close-to-passband TZs can be controlled independently for high selectivity. By adjusting the ratio of coupled and uncoupled lines in HLDR, the number of TZs in upper stopband is also controllable. To validate the proposed design method, one second-order 3.5 GHz and one 36 GHz BPFs are respectively designed with LTCC process. Very compact size, low loss, high-selectivity performance by TZs generation, and extended upper stopband can be simultaneously observed in the microwave and mm-wave bands.

The organization of this paper is given as below. The analyses of LTCC-based HLDR will be given in Section II. In Section III, the improved design method for HLDR bandpass filters with multiple TZs is investigated. Finally, one sub-6 GHz and one mm-wave LTCC filters are designed respectively for demonstrations in Section IV.

II. LTCC-BASED HYBRID LUMPED AND DISTRIBUTED RESONATORS

To begin with, the idea of the proposed hybrid resonator is introduced with an effective integrated design of the lumped elements and distributed effects. Second, the implementations of the proposed HLDR in LTCC process are investigated. At last, the characteristics of the proposed LTCC-based HLDR are analyzed.

A. INTEGRATED DESIGN FOR LTCC-BASED HLDR

As for reported mm-wave front-ends, BPFs were not applied due to its large circuit size and transmission loss. To solve this problem, the LTCC-based hybrid resonator is proposed by effectively utilizing the advantages of lumped and distributed elements.

Table 2 shows a comparison between lumped, distributed, mixed lumped-distributed BPFs and our proposed HLDR filters. First, the proposed HLDR can be regarded as an open-loop resonator in which the open ends are coupled with a lumped capacitor, as shown in Fig. 1. As the capacitance C_1 increases, the frequency-relevant open-loop resonator turns

TABLE 2. Comparison between the reported lumped, distributed, mixed lumped-distributed BPFs and proposed HLDR filter.

	Lumped filters [14]-[15]	Distributed filters [7]-[13]	Mixed lumped-distributed filters [18]-[22]	Proposed LTCC-based HLDR filter
Adopted resonator	Series or parallel *LC* ranks	Open-loop resonator, stub-loaded resonator, etc.	Distributed resonator loaded with chip capacitors	Integrated design of lumped elements and distributed effects
Circuit size of resonator	Frequency-irrelevant	$0.25\lambda g$ - $0.5\lambda g$	$< 0.25\lambda g$	$0.01\lambda g$ - $0.08\lambda g$
Inter-connection of resonators	Lumped elements	Mutual couplings	Lumped elements (mainly)	Mutual couplings

to one frequency-irrelevant HLDR. Therefore, HLDR is of very compact size, just like the lumped resonator. Second, the coupling effect of HLDR to the ground C_2 and to adjacent resonator are also considered, which make HLDR performs more than a parallel or series *LC* tank.

Besides the adopted resonator, the inter-connection way of resonators also determines filtering responses. As for lumped filters, the *LC* tanks were usually connected with lumped inductors or capacitors [14], [15]. Therefore, the design flexibility of lumped filters is limited by number of lumped elements. As for distributed filters, the coupling matrix method can be used, which is based on coupling coefficients of inter-resonators and external quality factors of the input and output resonators [7]. Therefore, high design flexibility was realized for the distributed filters [7]–[13]. As for our proposed HLDR bandpass filters, the mutual couplings between HLDRs, including both electric and magnetic couplings, are introduced by the coupled transmission lines. By appropriately adjusting the coupling matrix, the bandwidth and stopband performance of HLDR filters can be flexibly controlled.

In order to realize good performance in high frequency, especially in mm-wave band, HLDR is introduced with an effective integrated design of lumped components and distributed effects:

1) Lumped elements, namely the LTCC inter-digital capacitor and high-impedance microstrip section inductor, are used to realize compact size, low radiation loss, and low cross-talk;
2) Distributed effects, namely the mixed couplings, are introduced to improve the filtering performance. For example, the desired filtering responses can be realized based on coupling matrix method; multiple TZs are introduced in the stopband by using mixed couplings.

Compared with reported hybrid filters [18]–[22] and our previously work [24], both the compact size and good filtering response are obtained for the proposed HLDR filters, especially in mm-wave bands.

B. IMPLEMENTATION OF HLDR BY USING LTCC PROCESS

In the following, a compact HLDR is well implemented by making full use of the LTCC technology. The employed LTCC substrate is Ferro A6-M with dielectric constant

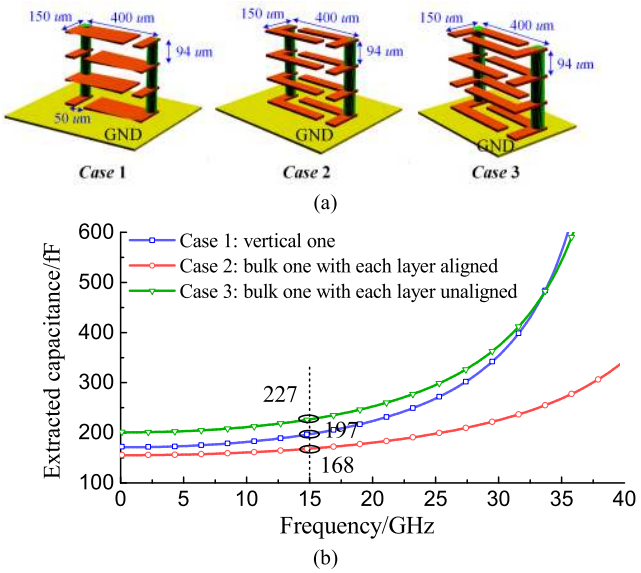

FIGURE 2. Three types of LTCC-based lumped capacitors with same circuit size. (a) *Case 1*: Vertical MIM capacitor [17], *Cases 2&3*: 3-D interdigital capacitors. (b) Extracted capacitances.

of 5.9 and loss tangent of 0.002. The thickness of each metal and dielectric layer is 10 um and 94 um, respectively. Compared with single-layer processes, the multi-layer LTCC process own several advantages:

(i) Large value of lumped capacitor can be realized with small circuit size by utilizing the couplings between the same and different layers;
(ii) Coupling topology of filter can be designed flexibly in multiple metal layers.

According to (i), the LTCC-based lumped capacitor can easily designed with compact size and large capacitance. As shown in Fig. 2(a), three cases of LTCC-based capacitors are analyzed, which are of same circuit size. By using electromagnetic (EM) simulation software, the impedance parameters of the LTCC-based capacitors can be obtained. The capacitances C_1 can be accordingly extracted by

$$C_1 = \frac{-1}{(\mathrm{im}(Z(1,1) + Z(2,2))) \times (\pi \times f)} \tag{1}$$

where im(Z(1,1)) and im(Z(2,2)) are the simulated impedance parameters, and f is the operating frequency.

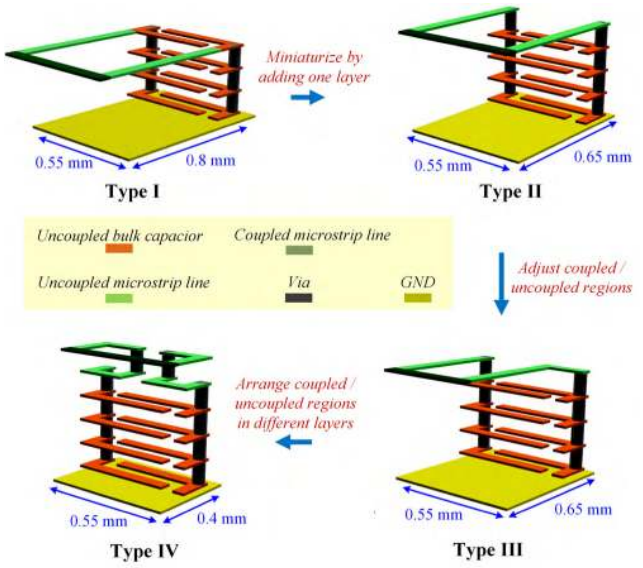

FIGURE 3. Flexible design of high-impedance microstrip section inductor in LTCC process for HLDR.

As shown in Fig. 2(b), the lumped capacitor in *Case 3* owns larger capacitance, because the couplings within the same layer and between different layers are both effectively utilized. Therefore, the LTCC-based lumped capacitor in HLDR is selected as *Case 3*.

Second, the high-impedance transmission line (TL) is also implemented with LTCC process, which has two functions: one is to provide the inductance for HLDR, and the other one is to introduce mutual coupling between adjacent resonators. As we see, the inductance of microstrip line can be calculated by [25]

$$L1(\text{nH}) = 2 \times 10^{-4} l \left[\ln\left(\frac{l}{w3+t}\right) + 1.193 + \frac{w3+t}{3l} \right] \times Kg$$
$$Kg = 0.57 - 0.145\ln(w3/h) \quad w3/h > 0.05 \tag{2}$$

where l and $w3$ is the length and width of the TL, respectively, t is the thickness of printed metallic layer, and h is the thickness of substrate. As for the microstrip line with complicated topology, the inductance L_1 can be obtained according to the simulations:

$$L_1 = \frac{\text{im}(Z(1,1) + Z(2,2))}{4\pi \times f} \tag{3}$$

In addition, the microstrip section inductors are used to introduce mutual couplings between adjacent HLDRs. According to (ii), the coupling topology of TL can be designed flexibly in LTCC process, as shown in Fig. 3. For Type I, the TL and lumped capacitor are connected directly on both sides; for miniaturization, the TL is placed above the interdigital capacitor in Type II; for Type III, the TL is folded, and ratio of coupled and uncoupled TLs can be adjusted; for Type IV, the uncoupled TL can be arranged in the lower metal layer beneath the coupled one. By using multi-layer LTCC process, a large freedom can be achieved to design the coupled and uncoupled TLs of HLDR, so as to the coupling coefficient between coupled HLDRs.

C. CHARACTERISTICS OF LTCC-BASED HLDR

As shown in Fig. 3, the resonant frequency of HLDR mainly depends on its self-capacitance C_1 and self-inductance L_1

$$f_0 \approx 1/(2\pi\sqrt{C1 \times L1}) \tag{4}$$

The mutual coupling between the microstrip section inductor and lumped capacitor is weak, therefore, the resonant frequency can be controlled independently by adjusting the dimensions of inductor and capacitor, respectively.

In addition, the total quality factor Q of microstrip resonator can be expressed by [26]

$$Q = [1/Qc + 1/Qd + 1/Qr]^{-1} \tag{5}$$

Here, Q_c, Q_d, and Q_r are the quality factors corresponding to conductor, dielectric, and radiation losses, respectively. Generally, the loss of resonator increases significantly with the smaller circuit size and higher operating frequency. Fortunately, with an effective integrated design of lumped and distributed elements, high quality factor is realized for the proposed compact LTCC-based HLDRs, which is obtained by the following techniques:

(1) Reduce radiation loss by using quasi-lumped interdigital capacitor and high-impedance microstrip line, especially in mm-wave band;
(2) Reduce dielectric loss by using smaller substrate due to the miniaturized LTCC-based HLDR;
(3) Avoiding increasing the conductor loss causing by inverse currents when miniaturizing the resonator.

For demonstration, the simulated resonant frequency and quality factor are given in cases of different dimensions of HLDR, as shown in Fig. 4. The circuit size of LTCC-based HLDR is about $0.005\times0.01\ \lambda_0^2$ in sub-6 GHz, while $0.03\times0.06\ \lambda_0^2$ in mm-wave band. Compared with distributed resonators, significant size reduction is realized. Furthermore, the resonant frequency and quality factor of HLDR can be easily controlled by adjusting its structural parameters, indicating large design flexibility remains to realize desired resonant frequency and bandwidth. At last, the quality factor increases rapidly with the operating frequency, therefore, the proposed HLDR is quite suitable for low-loss mm-wave bandpass filters.

III. DESIGN METHOD BASED ON FREQUENCY-VARIANT IN-PHASE MIXED COUPLINGS

For HLDR filters, the mutual couplings are introduced between adjacent resonators. Therefore, the widely used coupling matrix method for distributed filters can be applied. To improve selectivity and stopband suppression for BPFs, the generation of transmission zeroes (TZs) is significant.

To realize TZs, one common method is adding bandstop structures, such as open/shorted stubs [27], [28]. However, the circuit size and insertion loss of bandpass filters would increase if more TZs are desired.

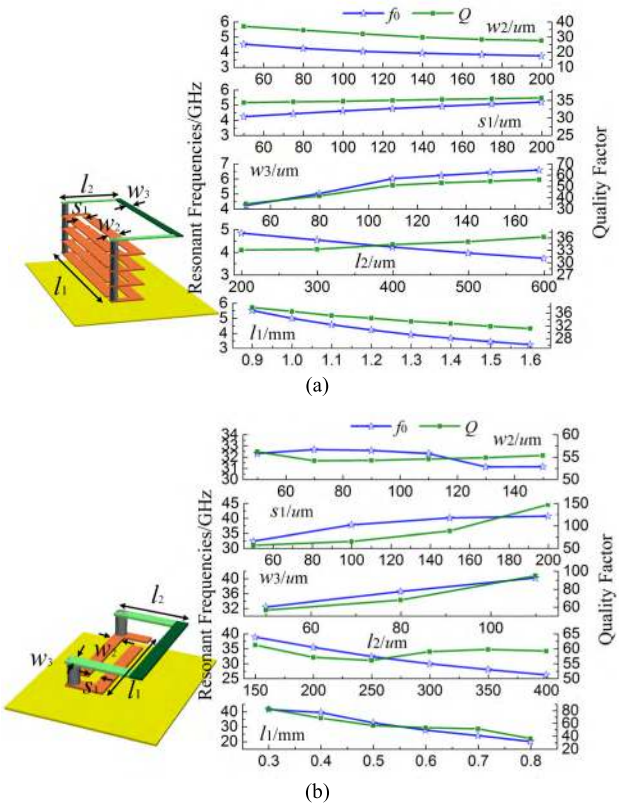

FIGURE 4. Topology of the proposed LTCC-based HLDR. Resonant frequency and quality factor of HLDR against its dimensions. (a) Sub-6 GHz HLDR. (Initial structural parameters: $w_2 = 80$, $w_3 = 50$, $s_1 = 50$, $l_1 = 1200$, $l_2 = 400$) (b) mm-wave HLDR. (Initial structural parameters: $w_2 = 50$, $w_3 = 50$, $s_1 = 50$, $l_1 = 500$, $l_2 = 250$) (Unit: *um*).

For the filters without bandstop structures, the TZs can be realized based on coupling matrix method, as listed in Table 3. For the filter with in-line topology, no TZs can be realized [7]. By adding cross couplings, two TZs are generated for the second-order [29], [30] or fourth-order filter [7]. Based on the out-of-phase mixed couplings [31]–[33], one TZ is realized for second-order filter, while two TZs are for the fourth-order one. Generally, it was quite difficult to realize multiple TZs for BPFs with simple structure.

In this paper, the coupling matrix method is improved by introducing a new coupling mechanism. The frequency-variant mixed couplings are investigated to realize multiple TZs. Different from [31]–[33], the mixed couplings exist in same coupling path; therefore, the electric and magnetic couplings are in-phase, as illustrated in Fig. 5(a). By only using a two-pole in-line topology, two controllable close-to-passband TZs can be realized for high selectivity. By adjusting the ratio of coupled and uncoupled lines in HLDR, the number of generated TZs in the upper stopband is also controllable.

A. REALIZATION OF TWO CLOSE-TO-PASSBAND TZS

As shown in Fig. 5(b), the electric coupling between adjacent microstrip lines is represented by a capacitance C_e, which is relevant to the coupled area and space of two TLs.

TABLE 3. Coupled-resonator bandpass filters with different coupling mechanisms (No bandstop structures).

Coupling mechanism	Order	Filter topology	Response $\|S_{21}\|$	Num. of TZs
Coupling matrix method with **in-line topology** [7]	Second-order	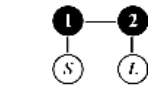	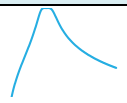	0
Coupling matrix method with **cross couplings** [7], [29]-[30]	Second-order	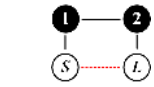 Source-load [29]-[30]	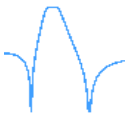	2
	Fourth-order	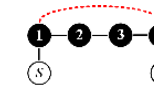 1st-4th resonators [7]	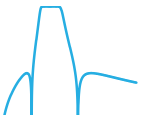	2
Coupling matrix method with ***out-of-phase*** **mixed couplings** [31]-[33]	Second-order	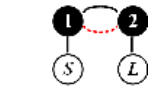	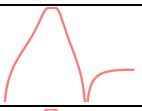	1
		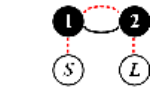	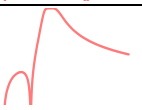	1
	Fourth-order	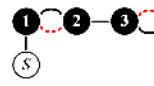	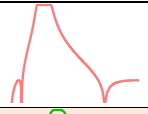	2
Coupling matrix method with **proposed *in-phase* mixed couplings**	Second-order	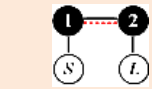	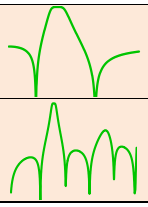	**2-6**

Dash line: electric coupling; solid line: magnetic coupling.

For the magnetic coupling coefficient k_m, it increases with larger ratio of coupled and uncoupled lengths of TL, and smaller space. Moreover, the outer-resonator coupling between ports and corresponding resonators is represented by C_q. Fig. 5(b) gives the *LC* equivalent circuit model of HLDR bandpass filter.C_c represents the electric coupling between adjacent interdigital capacitors. C_{gl}/C_{gc} is the coupling effect between inductor/capacitor and ground, while L_q represents the inductance of feeding line.

For this design, the TZs are generated due to the cancellation of the electric and magnetic couplings. For demonstration, the response of corresponding equivalent circuit is given in Fig. 5(c). We may see that, the two close-to-passband TZs are generated if C_c, C_e, and k_m are included in the equivalent circuit. Moreover, the two TZs will not disappear when removing the capacitors C_c or C_e. However, no TZ is realized if without both C_c and C_e. In addition, the left transmission zero TZ_1 can be mainly controlled by the capacitance C_e, as verified in Fig. 6(a). As shown in Fig. 6(b), the right transmission zero TZ_2 can be controlled by the capacitance C_c.

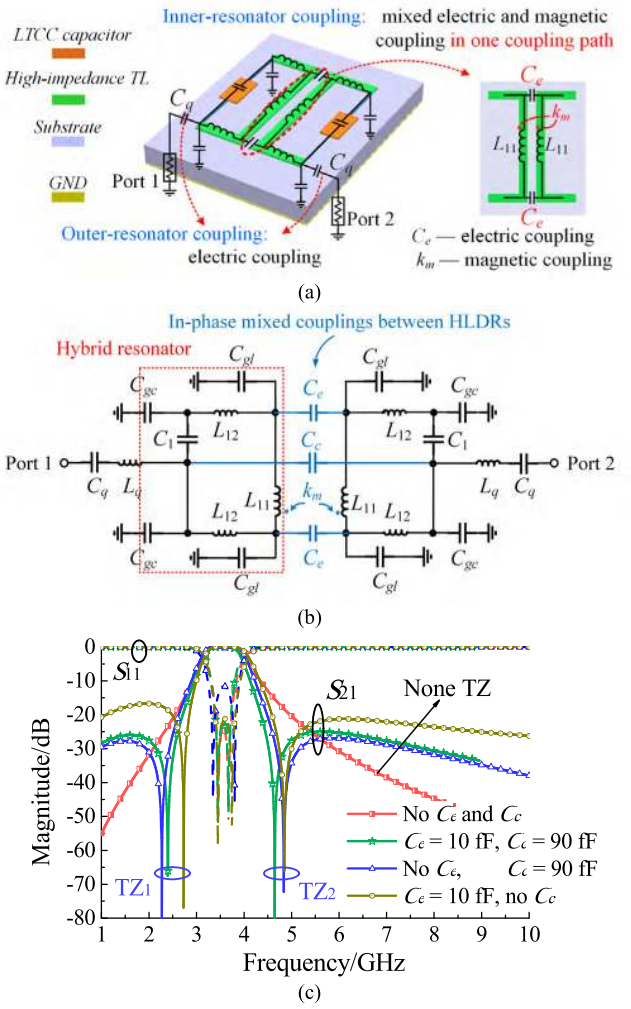

FIGURE 5. Second-order HLDR bandpass filters. (a) Coupling mechanism. (b) *LC* equivalent circuit. (c) Circuit simulations with or without TZs. Circuit parameters: $C_1 = 1130$, $C_{gl} = 250$, $C_{gc} = 418$, $C_q = 10$ (fF); $L_{11} = 0.37$, $L_{12} = 0.65$, $L_q = 1.15$ (nH); $km = 0.32$.

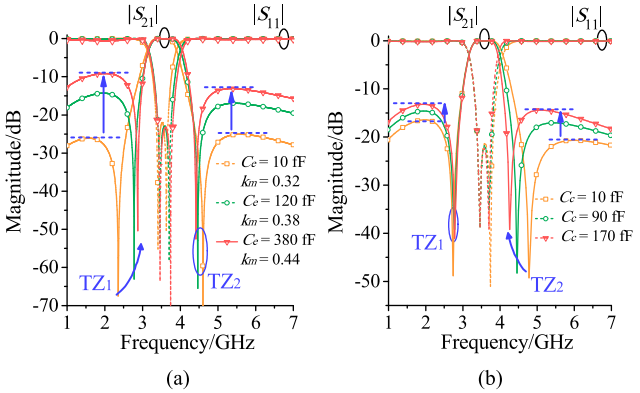

FIGURE 6. Controllable TZs and suppression level. (a) Controllable TZ_1 against electric coupling between coupled inductors C_e. (b) Controllable TZ_2 against electric coupling between adjacent capacitors C_c.

Meanwhile, the suppression level of HLDR bandpass filter can be improved with smaller C_c and C_e, which can be realized with the following solutions:

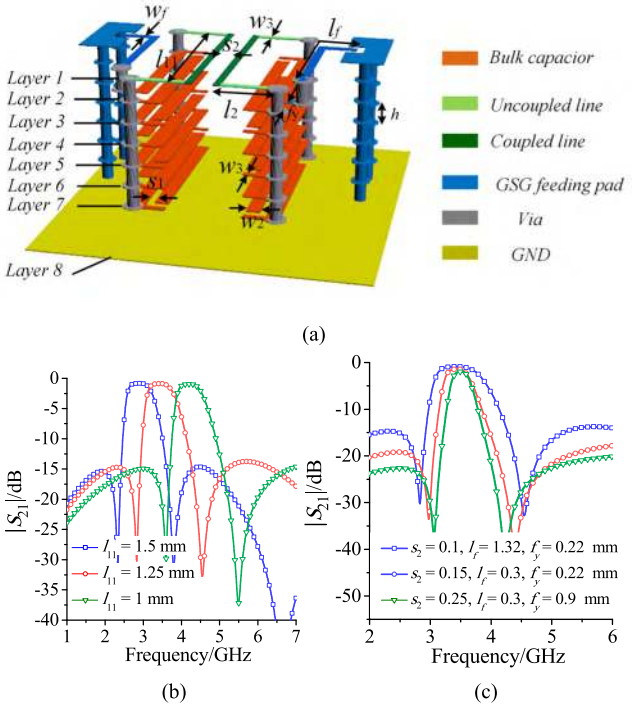

FIGURE 7. Proposed HLDR bandpass filter. (a) 3-D layouts. (b) Controllable center frequency. (c) Controllable bandwidth.

(a) Reduce C_c by enlarging the distance of adjacent inter-digital capacitors;
(b) Reduce C_e by decreasing the width w_3 and length l_{11} of coupled lines, and increasing the gap s_2 between adjacent coupled lines.

With the overall consideration of high stopband suppression and high selectivity for passband, an alternative solution is needed for HLDR bandpass filters.

Besides the newly introduced two TZs, the in-band performance of HLDR bandpass filter is designed based on coupling matrix theory [7]. First, a compact HLDR is designed according to the analyses in Section II. Furthermore, the bandpass design parameters can be calculated by

$$Q_{e1} = g_0 g_1 / FBW \quad Q_{e2} = g_1 g_2 / FBW$$
$$M_{12} = FBW / \sqrt{g_1 g_2} \tag{6}$$

A 3-D layout of the proposed LTCC bandpass filter is illustrated in Fig. 7(a). The external quality factors Q_{e1} and Q_{e2} mainly depend on the length l_f of feeding line and feeding position f_y. The coupling coefficient M_{12} is related to the gap s_2 and length l_{11} of coupled lines.

In addition, the center frequency and bandwidth of HLDR bandpass filters can be controlled flexibly. According to (2), the resonant frequency mainly depends on the capacitance C_1 and inductance L_1 ($L_{11} + L_{12} \times 2$). As illustrated in Fig. 7(b), the center frequency can be controlled by adjusting the structural parameters of adopted capacitor and inductor. Furthermore, a flexible bandwidth from 9.7% to 24% (associated insertion loss from −1.9 dB to −0.9 dB) can also be realized, as observed in Fig. 7(c).

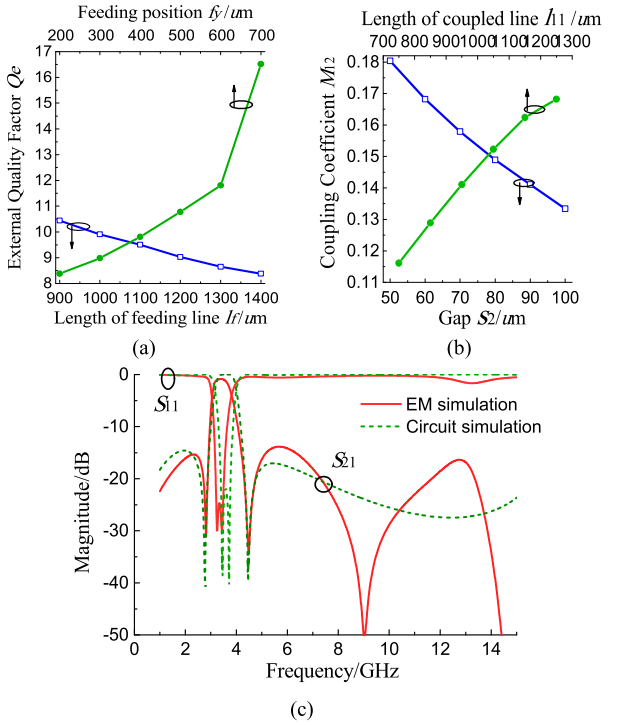

FIGURE 8. **Proposed sub-6 GHz HLDR bandpass filters (*Circuit I*). (a) Simulated external quality factors. (b) Simulated coupling coefficients. (c) EM and circuit simulations. Structural parameters: $w_f = 60$, $l_f = 1320$, $s_f = 50$, $f_y = 220$, $w_2 = 100$, $w_3 = 50$, $s_1 = 50$, $s_2 = 100$, $l_{11} = 1250$, $l_2 = 450$ (*um*).**

For experimental demonstration, a second-order bandpass filter with $f = 3.4$ GHz and FBW $= 22\%$ is desired (*Circuit I*). The capacitance C_1 is selected as 1130 fF, while inductance L_1 is chosen as 1.5 nH. Furthermore, the simulated Q_e and M_{12} can be extracted according to [7], as shown in Figs. 8(a)-(b). According to (4), l_f and f_y are selected as 1320 um and 220 um, respectively, while s_2 is equal to 100 um, and l_{11} is equal to 1250 um. The final structural parameters of HLDR bandpass filter are given in Fig. 8. The circuit size (not including GSG pad) is only $1.25\times1.3\times0.668$ mm^3 ($0.014\times0.015\times0.007$ λ_0^3). The EM and circuit simulated results are plotted in Fig. 8(c). We may see that center frequency is located at 3.4 GHz with 3-dB fractional bandwidth (FBW) of 22%, and the minimum insertion loss is only -0.87 dB. Two close-to-passband TZs can be observed, located at 2.82 and 4.48 GHz, respectively. However, the stopband rejection with 14 dB suppression till 15 GHz is not good enough.

As shown in Fig. 8(c), a good agreement can be observed between the EM and circuit simulations for in-band responses. For the out-of-band responses, the *LC* equivalent circuit cannot predict the TZs well. To address this issue, the transmission-line equivalent circuit is further investigated for the multiple TZs in the upper stopband.

B. REALIZATION OF MULTIPLE TZS WITH FREQUENCY-VARIANT MIXED COUPLINGS

For second-order bandpass filters, it was quite difficult to realize multiple TZs except adding the coupling paths or

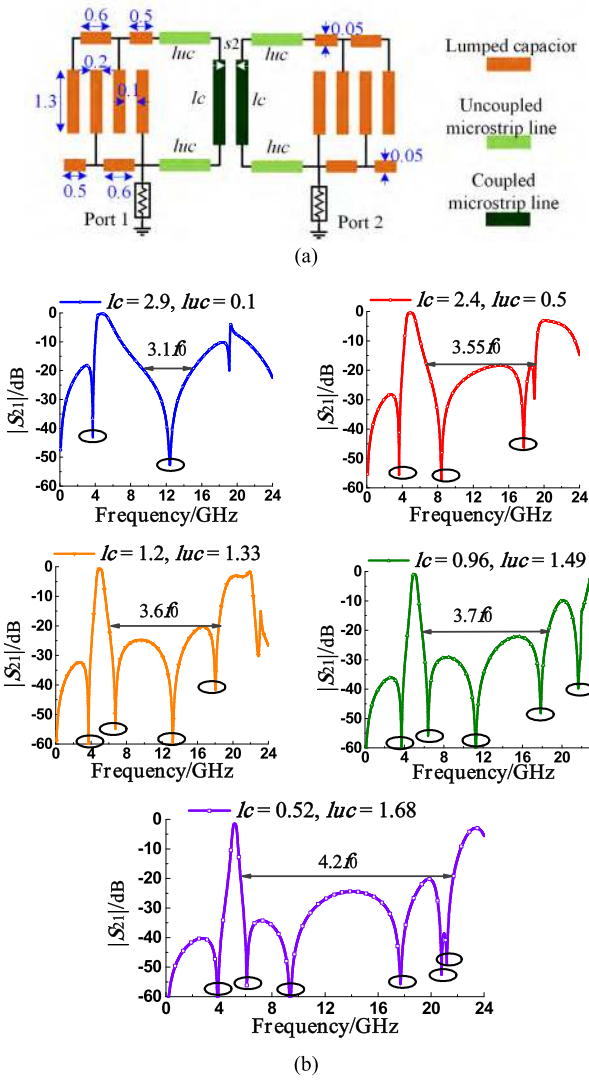

FIGURE 9. **Second-order HLDR bandpass filter. (a) Transmission-line equivalent circuit in Ansoft Designer (AD). (b) Circuit simulations against lengths of coupled transmission line l_c and uncoupled one l_{uc} (unit: mm).**

bandstop structures [27]–[30]. In [31]–[33], one or two TZs were realized based on out-of-phase mixed couplings. In this paper, the in-phase mixed couplings are investigated. Since the electric and magnetic couplings are frequency-variant, frequent cancellations can be realized for multiple TZs in the upper stopband.

As the frequency rises to upper stopband, the strengths of electric and magnetic couplings between HLDRs vary dramatically. Therefore, the proposed *LC* equivalent circuit is only valid for the in-band responses and two close-to-passband TZs. To further investigate the filter performance over a wide frequency range, the transmission-line equivalent circuit model is utilized, as illustrated in Fig. 9(a). As observed, each interdigital capacitor includes two pairs of fingers. The lengths of coupled and uncoupled TLs of each HLDR are represented by l_c and ($2\times l_{uc}$), respectively, and the ratio r_l is defined as ($0.5\times l_c/l_{uc}$).

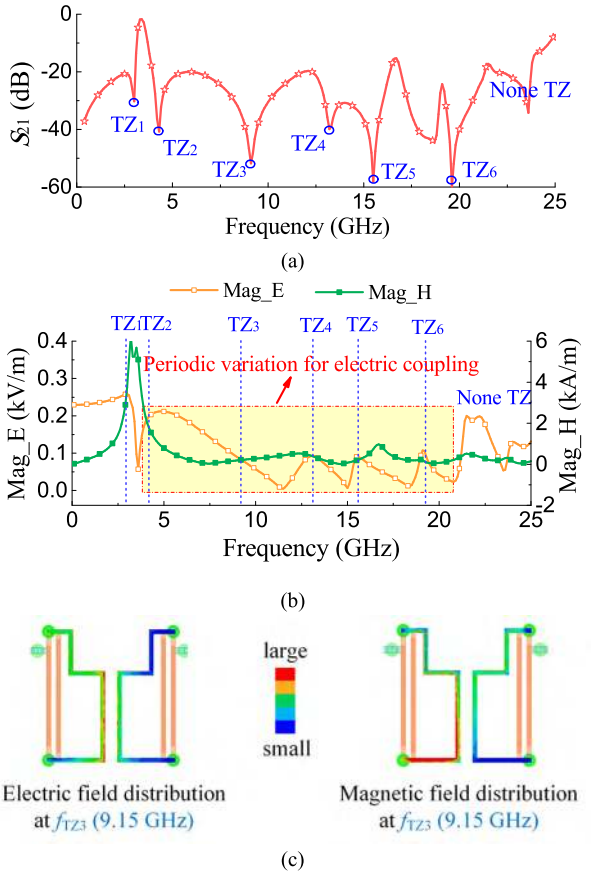

FIGURE 10. Explanation for the generation of TZs with mixed couplings. (a) Simulated response of an example with six TZs. (b) Electric and magnetic field intensities between adjacent HLDRs. (c) Electric and magnetic field distributions at the frequency of the third TZ.

The coupling mechanism of HLDR bandpass filter was introduced in Fig. 5. For the HLDR filter in Fig. 9(a), the electric coupling is relevant to the length l_c and space s_2, while the magnetic coupling increases with larger ratio r_l and smaller s_2. Therefore, the strengths of electric and magnetic couplings will change as the lengths l_c and l_{uc} vary, causing a different cancellation effect of the mixed couplings. As shown in Fig. 9(b), when the ratios rl is equal to 29, only two TZs can be observed at both sides of passband, resulting in 20 dB stopband suppression till $3.1f_0$ (see the first figure in Fig. 9(b)). When the ratio r_l decreases to 0.31, another four TZs are realized in the upper stopband, which significantly improves the out-of-band performance (see the last figure in Fig. 9(b)). Therefore, the number of TZs can be controlled from 2 to 6 for the second-order HLDR bandpass filter in Fig. 9(a).

For further explanation, six transmission zeroes are generated for an example of HLDR bandpass filter, as shown in Fig. 10(a). The electric and magnetic field intensities between adjacent HLDRs can be obtained by using field calculator in HFSS, as illustrated in Fig. 10(b). As observed, the magnetic field is quite large within the operating band, while remains a low value over the stopband. In term of electric field, four periodic variations can be observed from 5 GHz to 20 GHz. Therefore, four cancellations of the stable magnetic coupling and frequently varied electric coupling are realized, resulting in four TZs in the upper stopband. Therefore, the number of the generated TZs is controllable, and increases with the number of periodic variations of electric field between adjacent HLDRs. As shown in Fig. 10(c), the electric and magnetic field distributions are given at the frequency of the third TZ. Both electric and magnetic fields exist between HLDRs, which further demonstrate that the third TZ is realized with the cancellation of mixed couplings.

In conclusion, multiple TZs can be realized for a second-order in-line HLDR BPF by using frequency-variant mixed couplings. The two close-to-passband TZs can be easily controlled, while the number of generated TZs in the upper stopband is controllable. However, the bandwidth and insertion loss of bandpass filter will decrease with smaller r_l. In addition, aiming at compact size and low loss, no cross-couplings and bandstop structures are employed. Therefore, the structural parameters corresponding to TZs are few. To this end, only the number of generated TZs can be controlled, but not for the positions.

C. DESIGN PROCEDURE OF HLDR BPF WITH MULTIPLE TZS

Compared coupling matrix method [7], the out-of-band performance can be highly improved by using mixed couplings. The overall design procedures for LTCC-based HLDR filters can be summarized as follows:

step 1) Choose appropriate values for 3-D interdigital capacitor and microstrip section inductor according to filter specification. Reduce the circuit size and improve quality factor of HLDR. For example, set the spaces between adjacent fingers to 50 um in the same layer, and 94 um in different layers, use the minimum line width for microstrip lines;

step 2) Obtain the external quality factors Q_e and coupling coefficients M for HLDR bandpass filter according to coupling matrix theory;

step 3) Reduce the electric coupling between adjacent HLDRs to improve suppression level. Select appropriate lengths of coupled l_c and uncoupled l_{uc} lines to realize multiple TZs in the stopband;

step 4) Determine the feeding positions according to external quality factor Q_e. Determine the length and gap of coupled lines with the overall consideration of stopband performance and coupling coefficient M;

step 5) Obtain the final layout and dimensions for HLDR LTCC filter, and simulate the structure with full-wave simulation software.

IV. MICROWAVE AND MILLIMETER-WAVE LTCC-BASED HLDR BANDPASS FILTERS

In this section, one second-order S-band and one second-order Ka-band LTCC bandpass filters are designed for demonstration. Five TZs can be observed for the S-band filter but with relatively large insertion loss. Aiming at low-loss

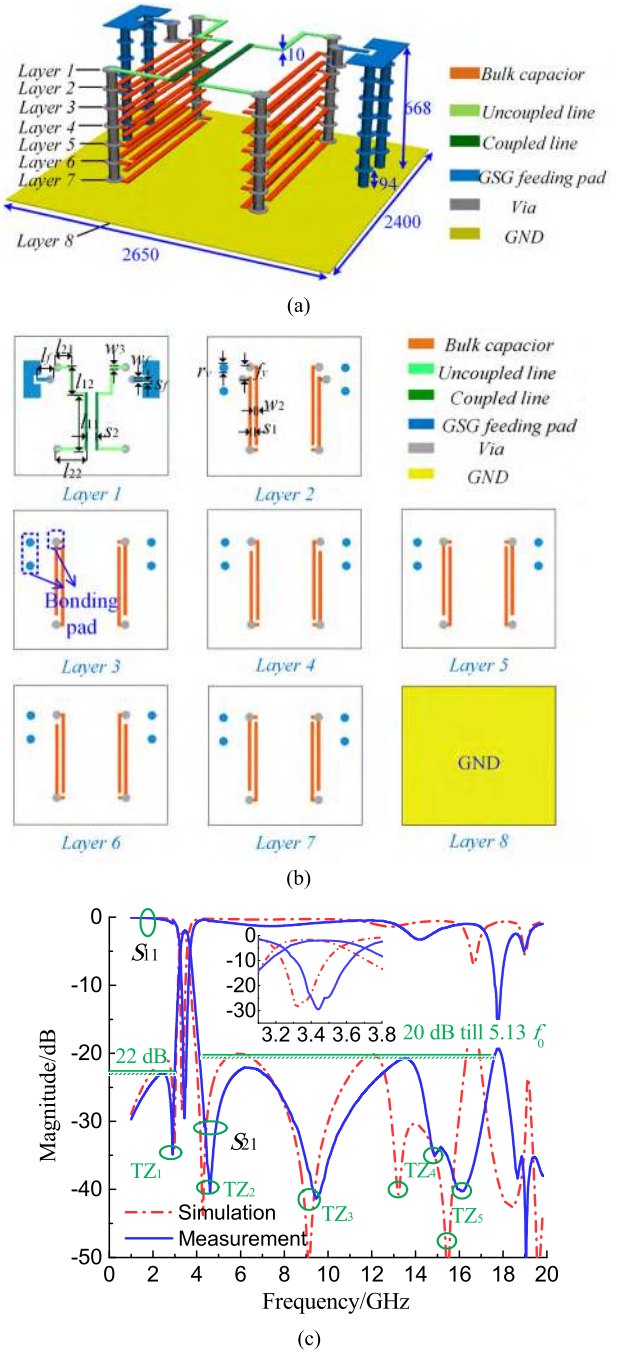

FIGURE 11. Proposed *S*-band HLDR bandpass filter (*Circuit II*). (a) 3-D layouts. (b) 2-D layouts. Dimensions: $f_y = 94$, $w_f = 60$, $s_f = 50$, $w_2 = 50$, $w_3 = 50$, $s_1 = 60$, $s_2 = 140$, $l_f = 350$, $l_{11} = 1030$, $l_{12} = 520$, $l_{21} = 300$, $l_{22} = 560$, $r_v = 145$. (Unit: *um*) (c) Measured and simulated results.

mm-wave HLDR filter, only four TZs is realized for the *Ka*-band filter.

A. S-BAND SECOND-ORDER HLDR BPF (CIRCUIT II)

The desired specification of second-order *S*-band bandpass filter is given as follows:

Passband: 3.2-3.6 GHz;

In-band return loss (*RL*): ≤ -20 dB;

Stopband: 20 dB suppression till 17 GHz ($5f_0$).

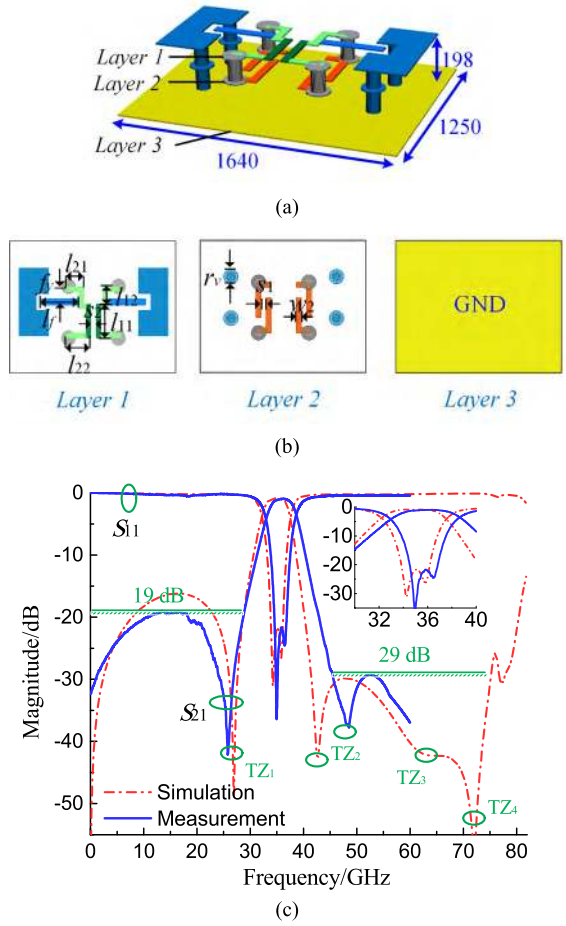

FIGURE 12. Proposed *Ka*-band HLDR bandpass filter (*Circuit III*). (a) 3-D layouts. (b) 2-D layouts. Dimensions: $f_y = 150$, $w_f = 60$, $s_f = 50$, $w_2 = 50$, $w_3 = 50$, $s_1 = 50$, $s_2 = 50$, $l_f = 380$, $l_{11} = 330$, $l_{12} = 170$, $l_{21} = 180$, $l_{22} = 250$, $r_v = 145$. (Unit: *um*) (c) Measured and simulated results.

According to the design procedure, the desired capacitance C_1 and inductance L_1 of HLDR are selected as 1400 fF and 1.7 nH, respectively. Furthermore, the design parameters of the filter can be obtained according to (4): $Q_{e1} = Q_{e2} = 11.7$, and $M_{12} = 0.089$. With the overall consideration of the following conditions:

(1) Inductances $L_{11} + L_{12} \times 2 = 1.7$ nH;

(2) Large l_{22} to realize small C_c (coupling between adjacent capacitors) for at least 20 dB suppression level;

(3) Small ratio of $l_{11}/(l_{12} + l_{21} + l_{22})$ for enough TZs to realize stopband suppression till 17 GHz;

(4) Appropriate length l_{11} to realize $M_{12} = 0.089$.

The lengths of the coupled and uncoupled inductors are determined as $l_{11} = 1030$ *um*, $l_{12} = 520$ *um*, $l_{21} = 300$ *um*, and $l_{22} = 560$ *um*. At last, the feeding position f_y, length l_f, and gap s_2 can be obtained based on the calculated Q_e and M_{12}. Based on [7], the extracted Qe and k are 13 and 0.087, respectively. The final layouts of the proposed *S*-band HLDR bandpass filter are given in Figs. 11(a) and (b), as well as the structural parameters. The core circuit size (not including G-S-G pad) is only $1.35 \times 1.59 \times 0.668$ mm^3 ($0.015 \times 0.018 \times 0.008\ \lambda_0^3$).

TABLE 4. Comparisons between the proposed HLDR bandpass filter and published sub-6 GHz bandpass filters.

Designs	Filter Type		Order	Center Frequency (GHz) / FBW	Insertion Loss/dB	Num. of TZs	Upper stopband Suppression	Circuit Size/ λ_0^3
[34]	PCB	MSL	3	2.1 / 19	-1.8	8	$3f_0$ (-18 dB)	0.26×0.26×0.007
[35]		SIW	3	3.7 / 6.7	-1.49	7	$2.65f_0$ (-20 dB)	0.24×0.5×0.012
[36]	LTCC	MSL	2	2.6 / 10.2%	-2.47	3	$4.1f_0$ (-28 dB)	0.017×0.015×0.017
[9]			2	2.4 / 11.5%	-2.59	4	$5.2f_0$ (-25 dB)	0.028×0.023×0.013
[37]		SIW	4	3.45 / 8.6%	-1.2	3	$2.38f_0$ (-19.8 dB)	0.2×0.16×0.009
*Circuit I**		HLDR	2	3.4 / 22.1%	-0.87	4	$4.4f_0$ (-14 dB)	0.014×0.015×0.007
Circuit II			2	3.47 / 12.6%	-1.90	5	$5.13f_0$ (-20 dB)	0.015×0.018×0.008

*Simulated results; MSL: microstrip line, SIW: substrate integrated waveguide

The measured and simulated results of the proposed LTCC bandpass filters are illustrated in Fig. 11(c). The measured results show that center frequency is located at 3.47 GHz with 3-dB fractional bandwidth (FBW) of 12.6%, the minimum insertion loss is −1.90 dB, and the return loss is better than −23 dB with two poles in the passband. Furthermore, five TZs can be observed in the stopband, located at 2.99, 4.6, 9.45, 15, and 15.91 GHz, respectively. With these TZs, a 20-dB stopband suppression is realized till $5.13f_0$.

B. KA-BAND SECOND-ORDER HLDR BPF (CIRCUIT III)

The desired specification of the second-order *Ka*-band bandpass filter is given as follows:

Passband: 32.5-37.5 GHz;
In-band return loss (*RL*): ≤ -20 dB;
Stopband: 20-dB suppression till 70 GHz ($2f_0$);
Minimum insertion loss: > -1 dB.

Compared with the *S*-band HLDR filter, we may see that the desired stopband suppression of *Ka*-band filter is only up to 70 GHz, but requesting lower insertion loss. As introduced in Section III-B, the number of TZs should be reduced to obtain the low-loss *K*a-band filter. Similarly, the desired C_1 can be obtained as 38 fF, while L_1 is 0.58 nH. According to (4), $Q_{e1} = Q_{e2} = 10$, and $M_{12} = 0.143$. With the overall consideration of insertion and stopband suppression, the lengths $l_{11,12,21,22}$ of coupled and uncoupled TLs can be determined. According to the calculated Q_e and M_{12}, the coupling parameters f_y, l_f, and s_2 can be obtained. From [7], the extracted Q_e and k are 11.8 and 0.134, respectively. The final layouts of the proposed *Ka*-band HLDR bandpass filter are given in Figs. 12(a) and (b), as well as its structural parameters. The core circuit size is only 0.64×0.64×0.198 mm^3 ($0.077\times0.077\times0.024\ \lambda_0^3$).

As shown in Fig. 12(c), the measured center frequency is located at 36.35 GHz with 3-dB FBW of 15.7%, the minimum insertion loss is −0.95 dB, and the return loss is better than −21 dB with two poles within passband. Four TZs can be observed from the simulated result, which can result in a 26-dB stopband suppression till 75 GHz. However, only two TZs can be observed from the measured results due to the frequency limitation of network analyzer and the adopted probes in the measurement.

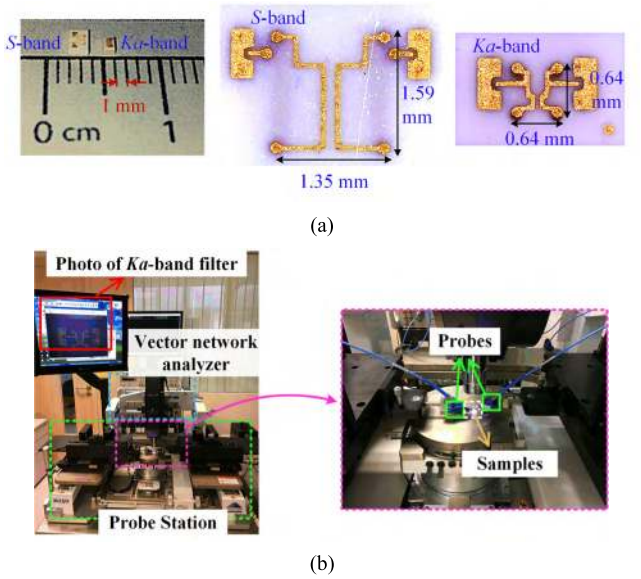

FIGURE 13. Photographs of (a) fabricated LTCC bandpass filters, (b) test platform with probe station.

C. RESULTS AND DISCUSSIONS

The electromagnetic simulation was carried out by using HFSS, while the measurement was made with an Agilent N5247A network analyzer. The photographs of fabricated samples are given in Fig. 13(a), while the test platform is shown in Fig. 13(b). Compared with the simulated results, a 2%-4% frequency shift of measured responses can be observed, which may be caused by fabrication tolerances of diameters of sintered metallic vias. Besides frequency shifts, the simulated/measured minimum insertion losses are 1.69/1.90, 0.85/0.95 dB for *Circuits II & III*, respectively. The additional 0.1-0.3 dB loss is attributed to the imperfect surface roughness of fabricated metal layers.

Table 4 shows the comparison between proposed *Circuits I& II* and several published sub-6 GHz filters. First, the proposed HLDR bandpass filters are most compact, especially

TABLE 5. Comparisons between the proposed HLDR bandpass filter and published planar mm-wave bandpass filters.

Designs	Filter Type		Order	Center Frequency (GHz) / FBW	Insertion Loss/dB	Num. of TZs	Stopband Suppression		Circuit Size/ λ_0^3
							Lower (dB)	Upper (dB)	
[38]	PCB	SIW	3	35 / 3.7%	-1.25	2		1.2f_0 (-40)	0.81×0.93×0.05
[10]	GaAs	MSL	2	60 / 25%	-1.2	2	till 0.75f_0 (-20)	1.43f_0 (-20)	0.1×0.08×0.02
[11]	CMOS		1	33 / 9.1%	-2.6	2	till DC (-20)	2.1f_0 (-20)	
[9]	LTCC	MSL	2	60 / 6.6%	-2.8	2	till DC (-32)	1.33f_0 (-28)	0.41×0.18×0.034
[39]		SIW	4	27.95 / 9%	-2.8	4		1.42f_0 (-20)	0.57×0.3×0.037
[40]			3	40 / 10.2%	-1.42	2		1.25f_0 (-25)	0.269×0.42×0.025
Circuit III		HLDR	2	36.35 / 15.7%	-0.95	4	till DC (-19)	[#]2.1 f_0 (-26)	0.077×0.077×0.02

[#] Measured responses are only available to 60 GHz, namely 1.65f_0 (-28 dB).

the *Circuit I*, 65% size reduction is obtained over the cited works. In addition, low insertion loss of −0.87 dB can be realized for *Circuit I*. Compared with *Circuit I*, the stopband suppression is much improved for *Circuit II*, but with slightly enlarged circuit size and insertion loss. In summary, *Circuit II* features compact size, low-loss, and wide stopband suppression.

Table 5 gives the comparison between *Circuit III* and other mm-wave bandpass filters. As observed, a very low insertion loss of −0.95 dB is realized at 36.35 GHz, which is better than the previously published filters with wider or narrower passbands. In addition, 95% size reduction is realized compared with cited LTCC mm-wave filters, and even smaller than the on-chip filters using gallium arsenide (GaAs) technology. At last, extended lower and upper stopband are realized for the proposed *Ka*-band HLDR filter.

V. CONCLUSION

A novel type of LTCC bandpass filters is proposed in this paper, featuring of low loss, very compact size, and wide stopband suppression, especially in mm-wave bands. First, an integrated design of lumped elements and distributed effects is realized, and the LTCC-based HLDR is proposed accordingly. As an improvement to coupling matrix method, the frequency-variant mixed couplings are investigated, which enables an easy realization of multiple TZs. For demonstration, two LTCC bandpass filters operating at 3.5 GHz and 36 GHz are designed and measured, respectively. Significant size reduction is realized compared with the cited works. The minimum insertion loss is only −0.95 dB at 36 GHz while with good selectivity and extended stopband. Owing to the above good features, the proposed design methodology can be applied for compact, low-loss, and wide-stopband bandpass filters from microwave to mm-wave bands.

REFERENCES

[1] T. S. Rappaport, S. Sun, R. Mayzus, H. Zhao, Y. Azar, K. Wang, G. N. Wong, J. K. Schulz, M. Samimi, and F. Gutierrez, "Millimeter wave mobile communications for 5G cellular: It will work!" *IEEE Access*, vol. 1, pp. 335–349, May 2013.

[2] X. Yi, G. Feng, Z. Liang, C. Wang, B. Liu, C. Li, K. Yang, C. C. Boon, and Q. Xue, "A 24/77 GHz dual-band receiver for automotive radar applications," *IEEE Access*, vol. 7, pp. 48053–48059, 2019.

[3] A. Heragu, D. Ruffieux, and C. Enz, "A low power BAW resonator based 2.4-GHz receiver with bandwidth tunable channel selection filter at RF," *IEEE J. Solid-State Circuits*, vol. 48, no. 6, pp. 1343–1356, Jun. 2013.

[4] A. E. Atia and A. E. Williams, "Narrow-bandpass waveguide filters," *IEEE Trans. Microw. Theory Techn.*, vol. 20, no. 4, pp. 258–265, Apr. 1972.

[5] B. Yassini and M. Yu, "Ka-band dual-mode super *Q* filters and multiplexers," *IEEE Trans. Microw. Theory Techn.*, vol. 63, no. 10, pp. 3391–3397, Oct. 2015.

[6] S. Moscato, C. Tomassoni, M. Bozzi, and L. Perregrini, "Quarter-mode cavity filters in substrate integrated waveguide technology," *IEEE Trans. Microw. Theory Techn.*, vol. 64, no. 8, pp. 2538–2547, Aug. 2016.

[7] J.-S. Hong and M. J. Lancaster, *Microstrip Filters for RF/Microwave Applications*. New York, NY, USA: Wiley, 2004.

[8] L.-H. Zhou and J.-X. Chen, "Differential dual-band filters with flexible frequency ratio using asymmetrical shunt branches for wideband CM suppression," *IEEE Trans. Microw. Theory Techn.*, vol. 65, no. 11, pp. 4606–4615, Nov. 2017.

[9] Q.-Y. Guo, X. Y. Zhang, L. Gao, Y. C. Li, and J.-X. Chen, "Microwave and millimeter-wave LTCC filters using discriminating coupling for mode suppression," *IEEE Trans. Compon., Packag., Manuf. Technol.*, vol. 6, no. 2, pp. 272–281, Feb. 2016.

[10] L.-P. Li, W. Shen, J.-Y. Ding, and X.-W. Sun, "Compact 60-GHz on-chip bandpass filter with low insertion loss," *IEEE Electron Device Lett.*, vol. 39, no. 1, pp. 12–14, Jan. 2018.

[11] Y. Zhong, Y. Yang, X. Zhu, E. Dutkiewicz, K. M. Shum, and Q. Xue, "An on-chip bandpass filter using a broadside-coupled meander line resonator with a defected-ground structure," *IEEE Electron Device Lett.*, vol. 38, no. 5, pp. 626–629, May 2017.

[12] S. Y. Zheng, Z. W. Liu, Y. M. Pan, Y. Wu, W. S. Chan, and Y. Liu, "Bandpass filtering Doherty power amplifier with enhanced efficiency and wideband harmonic suppression," *IEEE Trans. Circuits Syst. I, Reg. Papers*, vol. 63, no. 3, pp. 337–346, Mar. 2016.

[13] Y. Wu, L. Cui, W. Zhang, L. Jiao, Z. Zhuang, and Y. Liu, "High performance single-ended wideband and balanced bandpass filters loaded with stepped-impedance stubs," *IEEE Access*, vol. 5, pp. 5972–5981, 2017.

[14] R. Gómez-García, R. Loeches-Sánchez, D. Psychogiou, and D. Peroulis, "Single/multi-band Wilkinson-type power dividers with embedded transversal filtering sections and application to channelized filters," *IEEE Trans. Circuits Syst. I, Reg. Papers*, vol. 62, no. 6, pp. 1518–1527, Jun. 2015.

[15] Y. Yang, X. Zhu, E. Dutkiewicz, and Q. Xue, "Design of a miniaturized on-chip bandpass filter using edge-coupled resonators for millimeter-wave applications," *IEEE Trans. Electron Devices*, vol. 64, no. 9, pp. 3822–3828, Sep. 2017.

[16] S. Birgermajer, N. Janković, V. Radonić, V. Crnojević-Bengin, and M. Bozzi, "Microstrip-ridge gap waveguide filter based on cavity resonators with mushroom inclusions," *IEEE Trans. Microw. Theory Techn.*, vol. 66, no. 1, pp. 136–146, Jan. 2018.

[17] T. Yang, M. Tamura, and T. Itoh, "Super compact low-temperature co-fired ceramic bandpass filters using the hybrid resonator," *Microw. Theory Techn.*, vol. 58, no. 11, pp. 2896–2907, Nov. 2010.
[18] B. E. Carey-Smith, P. A. Warr, M. A. Beach, and T. Nesimoglu, "Wide tuning-range planar filters using lumped-distributed coupled resonators," *IEEE Trans. Microw. Theory Techn.*, vol. 53, no. 2, pp. 777–785, Feb. 2005.
[19] R. Zhang and D. Peroulis, "Mixed lumped and distributed circuits in wideband bandpass filter application for spurious-response suppression," *IEEE Microw. Wireless Compon. Lett.*, vol. 28, no. 11, pp. 978–980, Nov. 2018.
[20] A. Manchec, C. Laporte, C. Quendo, H. Ezzeddine, Y. Clavet, E. Rius, J.-F. Favennec, and B. Potelon, "Hybrid lumped/distributed band-pass filter in IPD technology for ultra-wideband applications," in *IEEE MTT-S Int. Microw. Symp. Dig.*, Jun. 2011, pp. 1–4.
[21] K. Ma, S. Mou, and K. S. Yeo, "Miniaturized 60-GHz on-chip multimode quasi-elliptical bandpass filter," *IEEE Electron. Devices Lett*, vol. 34, no. 8, pp. 945–947, Aug. 2013.
[22] Y.-H. Jeng, S.-F. R. Chang, and H.-K. Lin, "A high stopband-rejection LTCC filter with multiple transmission zeros," *IEEE Trans. Microw. Theory Techn.*, vol. 54, no. 2, pp. 633–638, Feb. 2006.
[23] R. J. Cameron, "General coupling matrix synthesis methods for Chebyshev filtering functions," *IEEE Trans. Microw. Theory Techn.*, vol. 47, no. 4, pp. 433–442, Apr. 1999.
[24] G. Shen, W. Che, W. Feng, and Q. Xue, "Analytical design of compact dual-band filters using dual composite right-/left-handed resonators," *IEEE Trans. Microw. Theory Techn.*, vol. 65, no. 3, pp. 804–814, Mar. 2017.
[25] I. Bahl, *Lumped Elements for RF and Microwave Circuits*. Norwood, MA, USA: Artech House, 2003.
[26] D. M. Pozar, *Microwave Engineering*. New York, NY, USA: Wiley, 2009.
[27] Y. Wu, Z. Zhuang, Y. Liu, L. Deng, and Z. Ghassemlooy, "Wideband filtering power divider with ultra-wideband harmonic suppression and isolation," *IEEE Access*, vol. 4, pp. 6876–6882, 2016.
[28] J. J. Sánchez-Martínez, M. Pérez-Escribano, and E. Márquez-Segura, "Synthesis of dual-band bandpass filters with short-circuited multiconductor transmission lines and shunt open stubs," *IEEE Access*, vol. 7, pp. 24071–24081, 2019.
[29] S. Amari, "Direct synthesis of folded symmetric resonator filters with source-load coupling," *IEEE Microw. Wireless Compon. Lett.*, vol. 11, no. 6, pp. 264–266, Jun. 2001.
[30] L. K. Yeung and K.-L. Wu, "A compact second-order LTCC bandpass filter with two finite transmission zeros," *IEEE Trans. Microw. Theory Techn.*, vol. 51, no. 2, pp. 337–341, Feb. 2003.
[31] K. Ma, J.-G. Ma, K. S. Yeo, and M. A. Do, "A compact size coupling controllable filter with separate electric and magnetic coupling paths," *IEEE Trans. Microw. Theory Techn.*, vol. 54, no. 3, pp. 1113–1119, Mar. 2006.
[32] S. Zhang and L. Zhu, "Synthesis design of dual-band bandpass filters with $\lambda/4$ stepped-impedance resonators," *IEEE Trans. Microw. Theory Techn.*, vol. 61, no. 5, pp. 1812–1819, May 2013.
[33] Y. He, G. Macchiarella, G. Wang, W. Wu, L. Sun, L. Wang, and R. Zhang, "A direct matrix synthesis for in-line filters with transmission zeros generated by frequency-variant couplings," *IEEE Trans. Microw. Theory Techn.*, vol. 66, no. 4, pp. 1780–1789, May 2018.
[34] K. D. Xu, F. Zhang, Y. Liu, and Q. H. Liu, "Bandpass filter using three pairs of coupled lines with multiple transmission zeros," *IEEE Microw. Wireless Compon. Lett.*, vol. 28, no. 7, pp. 576–578, Jul. 2018.
[35] W. Shen, "Extended-doublet half-mode substrate integrated waveguide bandpass filter with wide stopband," *IEEE Microw. Wireless Compon. Lett.*, vol. 28, no. 4, pp. 305–307, Apr. 2018.
[36] J.-X. Xu, X. Y. Zhang, X.-L. Zhao, and Q. Xue, "Synthesis and implementation of LTCC bandpass filter with harmonic suppression," *IEEE Trans. Compon., Packag., Manuf. Technol.*, vol. 6, no. 4, pp. 596–604, Apr. 2016.
[37] L.-S. Wu, X.-L. Zhou, W.-Y. Yin, L. Zhou, and J.-F. Mao, "A substrate-integrated evanescent-mode waveguide filter with nonresonating node in low-temperature co-fired ceramic," *IEEE Trans. Microw. Theory Techn.*, vol. 58, no. 10, pp. 2654–2662, Oct. 2010.
[38] X.-P. Chen and K. Wu, "Self-packaged millimeter-wave substrate integrated waveguide filter with asymmetric frequency response," *IEEE Trans. Compon., Packag., Manuf. Technol.*, vol. 2, no. 5, pp. 775–782, May 2012.
[39] K.-S. Chin, C.-C. Chang, C.-H. Chen, Z. Guo, D. Wang, and W. Che, "LTCC multilayered substrate-integrated waveguide filter with enhanced frequency selectivity for system-in-package applications," *IEEE Trans. Compon., Packag., Manuf. Technol.*, vol. 4, no. 4, pp. 664–672, Apr. 2014.
[40] S. W. Wong, R. S. Chen, K. Wang, Z.-N. Chen, and Q.-X. Chu, "U-shape slots structure on substrate integrated waveguide for 40-GHz bandpass filter using LTCC technology," *IEEE Trans. Compon., Packag., Manuf. Technol.*, vol. 5, no. 1, pp. 128–134, Jan. 2015.

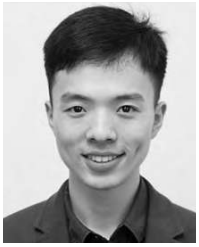

GUANGXU SHEN (S'15) was born in Jiangsu, China. He received the B.Eng. degree from the Nanjing University of Science and Technology (NUST), Nanjing, China, in 2014, where he is currently pursuing the Ph.D. degree with the Department of Communication Engineering.

From February 2014 to May 2014, he was an Exchange Student with the Institute of Nano-Electronics, Technische Universität München (TUM), Munich, Germany. From May 2017 to May 2018, he was a Research Assistant with the City University of Hong Kong. Since October 2018, he has been a Research Assistant with the South China University of Technology. His research interests include metamaterials and microwave/millimeter-wave passive circuits.

WENQUAN CHE (M'01–SM'11) received the B.Sc. degree from the East China Institute of Science and Technology, Nanjing, China, in 1990, the M.Sc. degree from the Nanjing University of Science and Technology (NUST), Nanjing, China, in 1995, and the Ph.D. degree from the City University of Hong Kong (CityU), Hong Kong, in 2003.

In 1999, she joined CityU, as a Research Assistant, where she was a Research Fellow and a Visiting Professor from 2005 to 2006 and 2009 to 2011. In 2002, she joined Polytechnique Montréal, Montréal, QC, Canada, as a Visiting Scholar. From 2007 to 2008, she was with the Institute of High Frequency Technology, Technische Universität München, Munich, Germany. From 2008 to October 2018, she was a Professor with the Nanjing University of Science and Technology. In November 2018, she joined the South China University of Technology, Guangzhou, China, where she is currently a Professor. She has authored or coauthored more than 300 internationally referred journal papers and international conference papers. Her research interests include electromagnetic computation, planar/coplanar circuits and subsystems in RF/microwave frequency, microwave monolithic integrated circuits (MMICs), and the medical application of microwave technology.

Dr. Che is a member of IEEE MTT-S AdCom Committee from 2018 to 2020. She was a recipient of the 2007 Humboldt Research Fellowship presented by the Alexander von Humboldt Foundation of Germany, the 5th China Young Female Scientists Award, in 2008, and the Distinguished Young Scientist received by the National Natural Science Foundation Committee (NSFC) of China, in 2012. He is an Associate Editor of the IEEE JOURNAL OF ELECTROMAGNETICS, RF, AND MICROWAVES IN MEDICINE AND BIOLOGY, and a Reviewer of the IEEE TRANSACTIONS ON MICROWAVE THEORY AND TECHNIQUES, the IEEE TRANSACTIONS ON ANTENNAS AND PROPAGATION, the IEEE TRANSACTIONS ON INDUSTRIAL ELECTRONICS, and the IEEE MICROWAVE AND WIRELESS COMPONENTS LETTERS.

QUAN XUE (M'02–SM'04–F'11) received the B.S., M.S., and Ph.D. degrees in electronic engineering from the University of Electronic Science and Technology of China (UESTC), Chengdu, China, in 1988, 1991, and 1993, respectively.

In 1993, he joined UESTC as a Lecturer, and later became a Professor in 1997. From 1997 to 1998, he was a Research Associate and then a Research Fellow with The Chinese University of Hong Kong, Hong Kong. In 1999, he joined the City University of Hong Kong, Hong Kong, where he was a Chair Professor of microwave engineering. From 2011 to 2015, he served the University as the Associate Vice President for Innovation Advancement and China Office, the Director for the Information and Communication Technology Center, and the Deputy Director for the State Key Laboratory of Millimeter Waves, Hong Kong. In 2017, he joined the South China University of Technology, Guangzhou, China, where he is currently a Professor and also the Dean of the School of Electronic and Information Engineering. He has authored or coauthored more than 300 internationally refereed journal papers and more than 130 international conference papers. He is a Co-Inventor of 5 granted Chinese patents and 15 granted U.S. patents, in addition with 26 field patents. His current research interests include microwave/millimeter-wave/terahertz passive components, active components, antenna, microwave monolithic integrated circuits, and radio frequency integrated circuits.

Dr. Xue was a recipient of the 2017 H. A. Wheeler Applications Prize Paper Award. He served for the IEEE as an AdCom Member of MTT-S from 2011 to 2013, an Associate Editor for the IEEE TRANSACTIONS ON MICROWAVE THEORY AND TECHNIQUES from 2010 to 2013, an Editor for the *International Journal of Antennas and Propagation* from 2010 to 2013, and an Associate Editor for the IEEE TRANSACTIONS ON INDUSTRIAL ELECTRONICS from 2010 to 2015. Since 2016, he has been an Associate Editor of the IEEE TRANSACTIONS ON ANTENNAS AND PROPAGATION.